Photoconductivity in single-crystal germanium sulphide

1990 J. Phys.: Condens. Matter 2 6195

(http://iopscience.iop.org/0953-8984/2/28/010)

J. Phys.: Condens. Matter **2** (1990) 6195–6205. Printed in the UK

Photoconductivity in single-crystal germanium sulphide

A M Elkorashy
Faculty of Engineering, Cairo University, Fayoum Branch, Fayoum, Egypt

Received 12 October 1989, in final form 9 January 1990

Abstract. The photoconductivity spectral response was measured for germanium sulphide (GeS) single crystals at different temperatures from room temperature to near liquid-nitrogen temperature. Measurements were carried out with plane-polarised light with the plane of polarisation parallel to the *a* and *b* crystallographic axes, which lie in the plane of cleavage. The photon energy range of measurements extended from 1.0 to 3.5 eV. The photoconductivity energy gap was determined from the spectral response by the Moss rule. The room-temperature photoconductivity energy gap was found to be 1.613 ± 0.010 and 1.642 ± 0.028 eV for the *a* and *b* axes, respectively. The temperature dependence of the photoconductivity energy gap was also deduced. It was found that it is linear between 92 and 300 K with a negative temperature coefficient equal to -0.43 ± 0.01 meV K^{-1} for the *a* axis. The results for the *b* axis showed a large discrepancy, which was attributed to crystal lattice bending introduced during the cleavage process. The minority-carrier lifetime was determined from the photoconductivity frequency response, which was found to be characterised by two different lifetimes.

1. Introduction

Germanium sulphide (GeS) is an interesting example of a layer-type semiconductor crystal. It has an orthorhombic structure with a D_{2h}^{16} space group. The atomic arrangement shows strongly distorted octahedral coordination, which causes considerable anisotropy of the physical properties. The lattice parameters of the GeS crystal were first determined by Zachariasen [1] as $a = 0.430$ nm, $b = 0.365$ nm and $c = 1.044$ nm. Here the *b* and *c* axes are inverted with respect to those of [1] to agree with current literature. The atomic coordination is 3 + 3 type with nearest-neighbour Ge–S distances 0.2441 nm (3×), 0.3270 nm (2×) and 0.3278 nm (1×) [2].

In previous work [3–5] the optical absorption in single-crystal GeS was studied near the fundamental absorption edge. The results were analysed on the basis of the two- and three-dimensional models. In another work [6] the optical constants of single-crystal GeS in the transparency region were also studied.

Investigations of photoelectric effects occupy an important place in studying the physical properties of semiconductors. They involve the study of photoconductivity and photoelectromotive forces. The aim of the present work is to present results on the photoconductivity of single-crystal GeS. In this respect we measured the photoconductivity spectral response, minority-carrier lifetime and the lux–ampere characteristic.

0953-8984/90/286195 + 11 $03.50

2. Experimental details

Undoped single crystals of GeS were grown by vapour transport in a temperature gradient, a method introduced by Schaefer [7] and modified by Hrubý [8]. The samples used in our measurements were prepared by cleavage from bulk or thicker single crystals. Samples of thickness ranging from 35 to 170 μm were used for photoconductivity measurements. In agreement with [9] and [10], we found that aquadag provided the most successful and reliable ohmic contacts. In order to improve the mechanical strength of the contacts and provide for easy wire-bonding, the aquadag contacts were covered with a layer of silver paste. Ohmic behaviour was verified by measuring the I–V characteristic, which was found to be linear up to the highest electric field used in our measurements. Moreover the I–V characteristic was found to be independent of the direction of the applied voltage.

To account for the anisotropy of the material, photoconductivity measurements were carried out with plane-polarised light with the plane of polarisation parallel to the a and b crystallographic axes, respectively, which lie in the plane of cleavage. We used a Leiss double monochromator with a Glan Thompson polariser. A tungsten precision lamp for optical devices was used as the light source. For photoconductivity measurements, we used square modulated illumination with a rise time between 0.2 and 0.4% of the pulse duration for different choppers. For lifetime measurements choppers of frequencies ranging from 3.0 to 700 Hz were used. The modulated illumination method has the advantage of eliminating the dark current, and the alternating component of the signal, which alone is measured, represents the value of the photocurrent. The sample is series-connected to a fixed resistor whose value is chosen to match the resistance of the sample. The DC bias is taken to correspond to the highest signal-to-noise ratio. The AC signal across the resistor is measured by a preamplifier connected to a lock-in amplifier that is engaged to a homodyne voltmeter. The use of a lock-in amplifier is essential for the measurements of very weak alternating signals of constant frequency, accompanied by heavy interference and noise background, which is the case.

The spectral range of measurements extended from 1.0 to 3.5 eV and the temperature was varied from room temperature to near liquid-nitrogen temperature. For low-temperature measurements, the sample holders were made of aluminium covered by aluminium oxide, which is a good heat conductor while being a good electrical insulator. In each holder a window of suitable dimensions was cut. The samples were mounted directly on the windows without any substrate to avoid the unnecessary complications introduced by the substrate.

The pronounced layer character of GeS poses some difficulties; for example we did not succeed in measuring the photoconductivity with the plane of polarisation parallel to the c crystallographic axis, which lies perpendicular to the plane of cleavage.

3. Method and results

3.1. X-ray study of crystal imperfections

Crystal imperfections are of special importance in the study of photoelectric properties of semiconductors. X-ray diffraction provides a powerful tool for the investigation of crystals and the study of their imperfections. Careful x-ray examinations of our samples

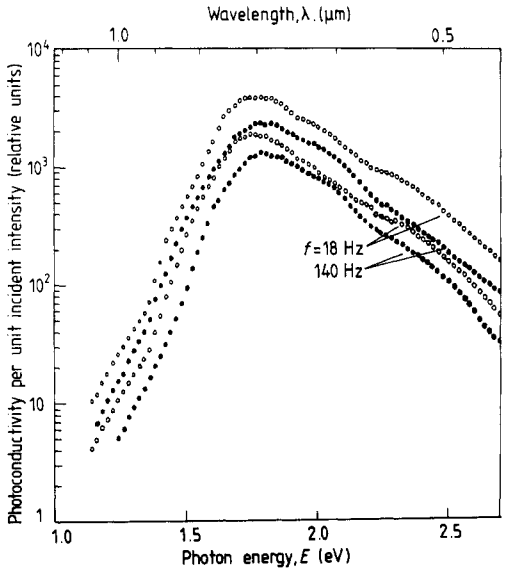

Figure 1. The spectral response of photoconductivity per unit incident intensity at room temperature and two different chopping frequencies: (○) *a* axis, (●) *b* axis.

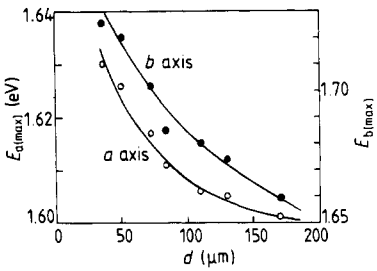

Figure 2. The variation of the photon energy corresponding to the maximum of the photoconductivity spectral response E_{max} with the sample thickness *d*.

were done by two methods, namely the back-reflection Laue photographs and the diffractometer method.

The Laue photographs showed elongated spots, which indicated bending of the lattice planes. By analysing the Laue spots we could see that the bending is about the *a* and *b* axes, but it predominates about the *a* axis. The length of the Laue streaks are a measure of the amount of bending that has occurred. We found that the radius of curvature corresponding to the largest amount of bending is about 9 mm. Such a high value of bending must be understood as local bending of the lattice planes.

The diffractometer patterns, which are usually called the rocking curves, indicated the presence of the kind of imperfection known as mosaic structure. The width of the rocking curve at zero intensities gave a maximum angle between the tiny blocks of the mosaic structure ranging from 1.8° up to 3.5°.

3.2. Photoconductivity spectral response

Figure 1 shows the photoconductivity spectral response normalised per unit incident intensity at room temperature and two different chopping frequencies (18 and 140 Hz). The figure shows that the response preserves its shape at the different frequencies; the maximum and characteristic breaks occur at the same values of photon energy. The photoconductivity spectral response of all samples exhibited clear maxima for both the *a* and *b* axes. The maximum is well defined for the *a* axis, while it is more or less flat for the *b* axis. The response decreased on both energy sides of the maxima, but the decrease was rapid towards the lower energy values and rather slow towards the higher energy values.

Table 1. The absorption coefficient at the maximum of the photoconductivity spectral response.

		a axis			*b* axis		
Sample No	d (μm)	E_{max} (eV)	α_i (cm^{-1})	$\alpha_i d$	E_{max} (eV)	α_i (cm^{-1})	$\alpha_i d$
1	35	1.630	443	1.55	1.726	411	1.44
2	49	1.626	351	1.72	1.720	371	1.82
3	72	1.617	186	1.34	1.702	258	1.86
4	83	1.611	125	1.04	1.685	166	1.38
5	109	1.606	88	0.96	1.680	148	1.61
6	130	1.605	86	1.12	1.674	131	1.70
7	170	1.601	72	1.22	1.659	83	1.41

Table 1 gives the photon energy of the maximum of the photoconductivity spectral response for the *a* and *b* axes, respectively, $E_{a(max)}$ and $E_{b(max)}$, and the corresponding interband absorption coefficients α_{ia} and α_{ib}. Table 1 also gives the product of the interband absorption coefficient and the thickness for the seven different samples that were used in our measurements. The photoconductivity spectral response shifts towards higher photon energies as the sample thickness decreases. Figure 2 shows the variation of the photon energy corresponding to the maximum of the photoconductivity spectral response E_{max} with the sample thickness d.

According to Moss [11] the spectral sensitivity $S(E)$, defined as $\Delta\sigma/\Delta\sigma_{max}$, is represented by the following expression:

$$S(E) = 1/\{1 + \exp[C(E_g - E)]\} \tag{1}$$

where C is a constant. From this expression we see that the spectral sensitivity falls to half (or the spectral response itself falls to half its maximum value) when the photon energy E is equal to the photoconductivity energy gap E_g^{photo}. This conclusion is known as the Moss rule.

The photoconductivity spectral response was measured at eight different temperatures from room temperature to 92 K. The response was then normalised per unit absorbed photon. Figure 3 shows the photoconductivity spectral response normalised per unit absorbed photon at the two extreme temperatures, namely 92 and 300 K for the *a* and *b* axes. The response at the other temperatures are not shown in the figure to avoid confusion. As the temperature was reduced, the maximum of the response increased in magnitude and its position shifted towards higher photon energies. The photoconductivity energy gap was determined from the spectral response normalised per unit absorbed photon at the eight different temperatures by applying the Moss rule. Figure 4 shows the temperature dependence of the photoconductivity energy gap for three samples that represent the maximum deviations in the value of the photoconductivity energy gap. The experimental points for the other samples lie between the broken curves in figure 4. From this figure it can be seen that the scattering of the experimental points corresponding to different samples is limited for the *a* axis but it is tremendous for the *b* axis. The room-temperature photoconductivity energy gap averaged over all samples is 1.613 ± 0.010 and 1.642 ± 0.028 eV for the *a* and *b* axes, respectively. From figure 4, it can be seen that the temperature dependence of the photoconductivity energy gap for

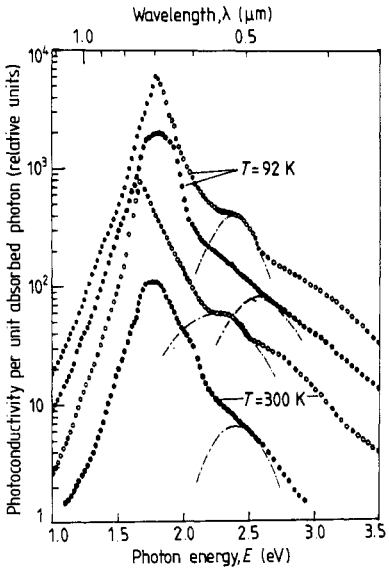

Figure 3. The photoconductivity spectral response normalised per unit absorbed photon at temperatures 92 and 300 K: (○) *a* axis, (●) *b* axis.

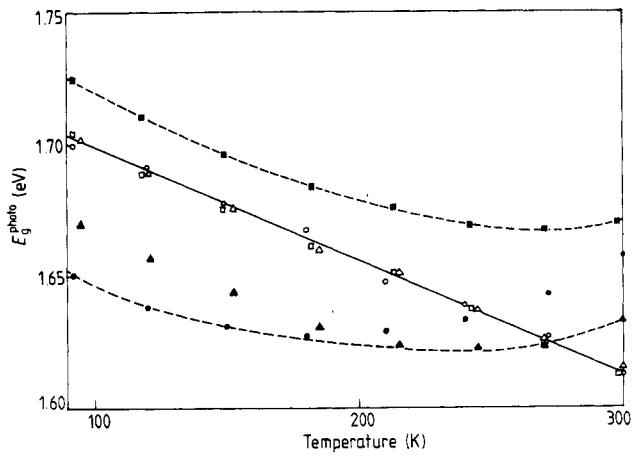

Figure 4. The temperature dependence of the photoconductivity energy gap: open symbols for *a* axis, full symbols for *b* axis.

the *a* axis is linear between 92 and 300 K with a negative temperature coefficient (dE_g^{photo}/dT) equal to -0.43 ± 0.01 meV K^{-1}. The case is different for the *b* axis, where the experimental points could not be connected by any straight line.

From figure 3, it is clear that the photoconductivity spectral response exhibits several characteristic breaks and could, therefore, be decomposed into several component bands whose superposition results in the original response. The activation energy of each component band could be determined by applying the Moss rule to each one separately. As a demonstration we tried to apply this procedure to figure 3 by decomposing the response into two components only, which are more clearly separable. The activation energy of this secondary band was found to be about 1.86 and 2.14 eV for

Table 2. Comparison between photoconductivity and optical energy gap values.

Physical quantity	Optical (indirect forbidden transition)					
	Two-dimensional		Three-dimensional		Photoconductivity	
	a axis	*b* axis	*a* axis	*b* axis	*a* axis	*b* axis
Energy gap E_g (eV) at room temp.	1.544 ±0.011	1.572 ±0.014	1.540 ±0.011	1.550 ±0.012	1.613 ±0.010	1.642 ±0.028
Temp. coeff. dE_g/dT (meV K^{-1})	−0.54	−0.63	−0.52	−0.60	−0.43	–
Phonon energy (meV)	22	26	20	22	–	–

the *a* and *b* axes, respectively, at room temperature, and about 2.16 and 2.30 eV, respectively, for the same axes at 92 K.

Table 2 shows a comparison between the photoconductivity and the optical energy gap values. The values of the optical energy gap are taken from [5].

3.3. Minority-carrier lifetime

This is the lifetime that is the key parameter in the photoelectric analysis. The details of the recombination mechanisms manifest themselves through the lifetime of the free carriers. The lifetime was determined from the photoconductivity frequency response (photoconductivity dependence on the chopping frequency). It was observed that, as the chopping frequency was reduced even up to 3.0 Hz, the photoconductivity was still increasing. It was therefore necessary to measure the steady-state photoconductivity by the method of continuous illumination using a sensitive compensator to be able to interpret the photoconductivity frequency response in a better way. Unfortunately, the method of continuous illumination has the disadvantage that the sample is continuously subjected to the illumination and consequently it is heated up, especially under illumination by infrared light. Heating the sample will also change its conductivity due to thermal generation of free carriers. The compensated voltage will, therefore, be due to the overall change in conductivity by the absorbed photons and by heating. This problem was studied in detail. The total change in conductivity was measured as a function of time.

Figure 5 shows the total change in conductivity as a function of time for two values of incident intensity. As the illumination was switched on, the conductivity increased rapidly and then more slowly. The lower incident intensity, which was only 6% of the higher one, was assumed to produce a much lower heating. Moreover, the sign of the change in conductivity due to heating alone was checked in darkness and it was found that in a narrow temperature range above room temperature the conductivity increased as the temperature was increased. This means that the conductivity increased both due to absorption of photons and due to heating. The rapid increase in conductivity was, therefore, attributed to photon absorption, i.e. photoconductivity, and the slow increase to heating. By this method we were able to separate the photoconductivity part from the total change in conductivity.

Figure 6 shows the photoconductivity frequency response at room temperature and photon energies 1.55, 1.65 and 2.20 eV for both the *a* and *b* axes including the steady-state

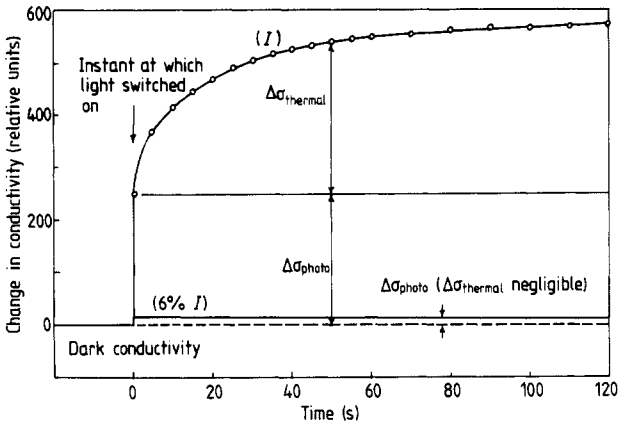

Figure 5. The total change in conductivity as a function of time.

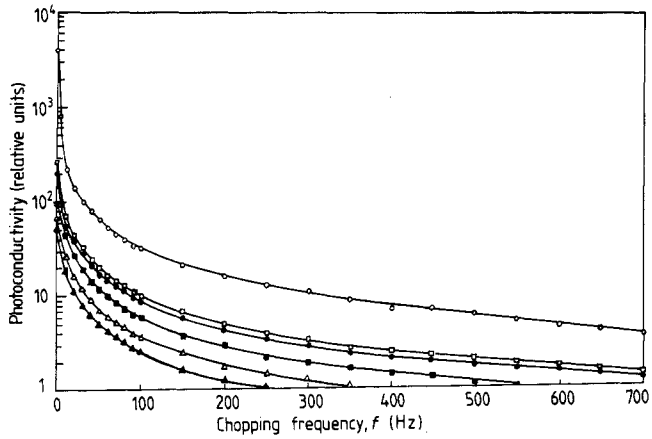

Figure 6. The photoconductivity frequency response at room temperature (T = 300 K) and different photon energies: open symbols for a axis, full symbols for b axis; E = 1.55 eV (squares), 1.65 eV (circles), 2.20 eV (triangles).

photoconductivity measured by the method explained above. For square modulated illumination the photoconductivity frequency response has the form [12]:

$$\Delta\sigma_{alt} = \Delta\sigma_{st}[\tanh(1/4\tau f)] \tag{2}$$

where $\Delta\sigma_{alt}$ is the amplitude of the alternating component of photoconductivity, $\Delta\sigma_{st}$ is the steady-state photoconductivity, f is the chopping frequency and τ is the lifetime.

Unfortunately there existed no function of the form (2) that could fit the experimental results over the whole range of chopping frequency. We were able to obtain a better fitting of our results by an equation of the form:

$$\Delta\sigma_{alt} = \Delta\sigma_{st(1)}[\tanh(1/4\tau_1 f)] + \Delta\sigma_{st(2)}[\tanh(1/4\tau_2 f)] \tag{3}$$

with two different values of lifetime τ_1 and τ_2.

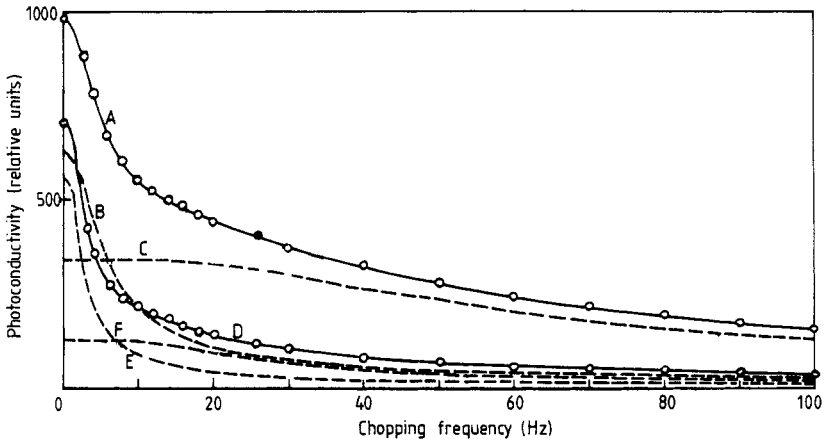

Figure 7. The photoconductivity frequency response for the *a* axis at $E = 1.65$ eV and $T = 92$ (A, B, C) and 300 K (D, E, F), demonstrating the fitting of the experimental results to equation (3). A: $\Delta\sigma = 618 \tanh 10^3/4 \times 70f + 340 \tanh 10^3/4 \times 6f$; B: $\Delta\sigma = 618 \tanh 10^3/4 \times 70f$; C: $\Delta\sigma = 340 \tanh 10^3/4 \times 6f$; D: $\Delta\sigma = 840 \tanh 10^3/4 \times 230f + 130 \tanh 10^3/4 \times 14f$; E: $\Delta\sigma = 840 \tanh 10^3/4 \times 230f$; F: $\Delta\sigma = 130 \tanh 10^3/4 \times 14f$.

Table 3. The short and long lifetimes for one sample.

Temperature (K)		92			300		
Photon energy (eV)		1.55	1.65	2.20	1.55	1.65	2.20
Short lifetime (ms)	*a* axis	6	6	6	14	14	14
	b axis	6	6	6	14	14	14
Long lifetime (ms)	*a* axis	45	70	60	190	230	90
	b axis	40	100	30	100	80	90

Figure 7 shows the photoconductivity frequency response (only up to 100 Hz) for the *a* axis at photon energy 1.65 eV at the two temperatures 92 and 300 K to demonstrate how the experimental results were fitted to equation (3). The best fitting of the experimental points in figure 7 is by the following expressions ($\Delta\sigma$ in relative units):

$$\Delta\sigma = 618 \tanh(10^3/4 \times 70f) + 340 \tanh(10^3/4 \times 6f) \qquad \text{for } T = 92 \text{ K}$$

$$\Delta\sigma = 840 \tanh(10^3/4 \times 230f) + 130 \tanh(10^3/4 \times 14f) \qquad \text{for } T = 300 \text{ K}.$$

Table 3 gives the values of the short and long lifetimes for one sample at the two extreme temperatures 92 and 300 K.

3.4. Lux–ampere characteristic

Figure 8 shows the lux–ampere characteristic for the *a* axis at photon energies 1.55, 1.65 and 2.20 eV at temperatures 92 and 300 K. The value $E = 1.55$ eV is near the fundamental absorption edge, while $E = 1.65$ eV corresponds to the position of the

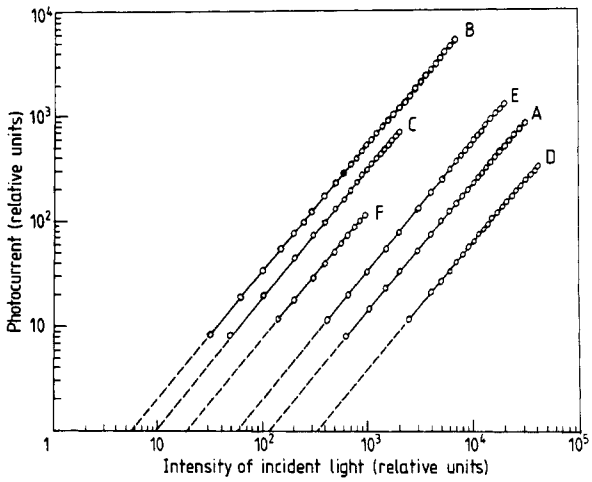

Figure 8. The lux–ampere characteristic for the *a* axis: curves A, B and C at $T = 92$ K and $E = 1.55, 1.65$ and 2.20 eV, respectively; curves D, E and F at $T = 300$ K and $E = 1.55, 1.65$ and 2.20 eV, respectively.

maximum of the photoconductivity spectral response at room temperature, and $E = 2.20$ eV is far above it. Similar results are obtained for the *b* axis. It can, therefore, be seen that the lux–ampere characteristic is linear for the three values of photon energy and all temperatures from 92 to 300 K up to approximately four orders of incident light intensity.

4. Discussion of results and conclusions

In measuring the amount of bending from the length of the Laue streaks, it must be remembered that the wavelengths present in the incident x-ray beam do not cover an infinite range. There is no radiation of wavelength shorter than the short-wavelength limit, and on the long-wavelength side the intensity decreases continuously as the wavelength increases. This means that, for a given degree of lattice bending, some Laue streaks may not be as long as they might be if a full range of wavelengths was available. The amount of bending estimated from the length of these streaks would therefore be smaller than that actually present. Thus, the information that we obtained about the degree of bending from such Laue photographs is, unfortunately, only relative and approximate. It can be assumed that this bending of the lattice planes was introduced into the samples during the cleavage process. This is because the bending predominates about the *a* axis, which is less inclined to the direction of cleavage. We could also assume that the mosaic structure imperfection was also introduced into the samples during the cleavage process.

The measured photoconductivity spectral response was more or less complicated, mainly because of the pronounced structure that was observed at different photon energies below and above the fundamental absorption edge. It was found that, as chopping frequency changed, the photoconductivity spectral response preserved its shape with its detailed structure. This led us to the conclusion that our results concerning

photoconductivity energy gap obtained by applying the Moss rule are independent of chopping frequency.

The photoconductivity spectral response increases as the photon energy increases up to energies slightly above the energy gap where it exhibits a maximum, then it decreases for larger photon energies. De Vore [13] has analysed the problem in terms of the absorption coefficient and the surface and volume recombination rates. The maximum usually occurs for an interband absorption coefficient α_i approximately equal to the reciprocal thickness $1/d$. In other words, the maximum usually occurs at a photon energy where $\alpha_i d$ is approximately equal to unity. This agrees fairly well with our results. From table 1, it can be seen that the location of the maximum of the response is located at photon energies where $\alpha_i d$ range from 0.96 to 1.72 for the *a* axis and from 1.38 to 1.86 for the *b* axis.

The averaged photoconductivity energy gap at room temperature as calculated from the normalised photoconductivity spectral response per unit absorbed photon was found to be 1.613 ± 0.010 and 1.642 ± 0.028 eV for the *a* and *b* axes, respectively. By comparing these values with the optical energy gap of the indirect forbidden transition at room temperature, as given in table 2, we see that the photoconductivity energy gap is higher than the two-dimensional optical energy gap by 69 and 70 meV for the *a* and *b* axes, respectively, and higher than the three-dimensional optical energy gap by 73 and 92 meV, respectively, for the same axes. The absolute value of the temperature coefficient of the photoconductivity energy gap for the *a* axis is smaller than that of the optical energy gap by 11 meV K^{-1} (two-dimensional) and 9 meV K^{-1} (three dimensional). The discrepancy is tremendous for the *b* axis. The results of the photoconductivity energy gap for the *b* axis are neither consistent for the different samples nor in agreement with those of the optical energy gap. The discrepancy can be mainly attributed to crystal imperfections, which influenced the results obtained by the application of the Moss rule, which holds, in principle, for perfect materials. Bending of the crystal lattice may be considered as the most important type of crystal imperfection influencing the results of photoconductivity, particularly because the thinnest samples had the highest photosensitivity and those were more subjected to bending. From our results on x-ray studies of the crystal imperfection, we found that bending is predominant about the *a* axis. This means that the change in the lattice parameter *b* is larger than that in the lattice parameter *a*. This fact may explain, at least qualitatively, the large disagreement of the photoconductivity and optical energy gaps for the *b* axis. It can also explain the inconsistency of the results of different samples for the *b* axis, as the amount of bending is different for each sample. On the other hand, samples used for optical measurements were relatively much thicker or even bulk. Moreover, it should be emphasised that the determination of the photoconductivity energy gap by the Moss rule does not take into consideration the phonon energy, which plays an important role in the precise determination of the optical energy gap.

Štourač *et al* [14], using unpolarised light, deduced that the photoconductivity energy gap of crystalline GeS depends on the crystal thickness, giving 1.35 and 1.5 eV for thickness 0.6 and 0.01 cm, respectively. Because these results are an unknown combination of the photoconductivity profiles for the two polarisation directions, they cannot serve for quantitative purposes. Taking into consideration that in [14] the samples used were much thicker than those in this work, together with the fact that unpolarised light was used, their results can be compared with ours.

From figure 3, it is clear that the response exhibited several characteristic breaks. The pronounced structure in photoconductivity spectral response led us to believe that

the response is the resultant of several component responses superimposed on each other. The Moss rule applies fairly well to each component separately, and the activation energy can be found for each band. Such a procedure has been described by Moss [11]. We applied this procedure and decomposed the response into the most two clear bands for the *a* and *b* axes. The activation energy of the secondary band was found to be approximately 1.86 and 2.14 eV at room temperature for the *a* and *b* axes, respectively, and 2.16 and 2.30 eV, respectively, at 92 K for the same axes. Kannewurf and Cashman [15] applied the same procedure for GeSe with unpolarised light. It should be emphasised that separation of component bands cannot be done in a unique way, particularly if the overlapping of two or more sub-bands is large enough. Therefore, such results concerning sub-bands must be considered as only approximate. For this reason we did not try to analyse the results in this way and decompose the whole photoconductivity response at all values of photon energy and temperature.

The interpretation of the results of lifetime measurements is rather difficult. We cannot draw a concrete conclusion about the recombination process on the basis of the present measurements alone. The short lifetime was found to be independent of photon energy and to have the value 14 ms at room temperature, which decreases to 6 ms at 92 K, and to be the same for the *a* and *b* axes. On the other hand, the long lifetime was found to be dependent on photon energy. The dependence changes from one sample to another. The value of the long lifetime is also different for the two considered axes. The value of the long lifetime at room temperature was found to vary between 75 and 250 ms for the *a* axis, and between 65 and 110 ms for the *b* axis for all samples. Moreover, the long lifetime generally decreased as the temperature decreased. From above discussions, it may be thought that the short lifetime is the one that is inherently dependent on the material itself while the long lifetime is strongly dependent on the sample conditions.

The linearity of the lux–ampere characteristic as shown from figure 8 may indicate the presence of one principal type of recombination centre. No definite information about it could be drawn on the basis of the present results alone.

References

[1] Zachariasen W H 1932 *Phys. Rev.* **40** 917
[2] Bissert G and Hesse K F 1978 *Acta Crystallogr.* B **34** 1122
[3] Elkorashy A M 1985 *Egypt. J. Solids* **7** 13
[4] Elkorashy A M 1986 *Egypt. J. Phys.* **17** 29
[5] Elkorashy A M 1988 *J. Phys. C: Solid State Phys.* **21** 2595
[6] Elkorashy A M 1989 *Physica* B **159** 171
[7] Schaefer H 1962 *Chemische Transportreaktionen* (Weinheim: Verlag Chemie)
[8] Hrubý 1975 *Czech. J. Phys.* B **25** 1413
[9] D'Amboise T, Handfield G and Bourgon M 1968 *Can. J. Phys.* **46** 3545
[10] Wiley J D, Pennington S and Schonherr 1979 *Phys. Status Solidi* b **96** K37
[11] Moss T S 1952 *Photoconductivity in the Elements* (London: Butterworths)
[12] Ryvkin S M 1964 *Photoconductivity Effects in Semiconductors* (New York: Consultants Bureau) p 40
[13] De Vore H B 1956 *Phys. Rev.* **102** 86
[14] Štourač L, Závětová M and Abrahám A 1974 *Proc. 12th Int. Conf. on Physics of Semiconductors (Stuttgart, 1974)* (Stuttgart: Teubner) p 1012
[15] Kannewurf C R and Cashman R J 1961 *J. Phys. Chem. Solids* **22** 293